JOURNAL OF MATERIALS SCIENCE 33 (1998) 4447–4453

Oxide and interface characteristics of oxidized silicon oxynitride ceramics – an investigation by electron microscopy

D. MANESSIS, HONGHUA DU
Stevens Institute of Technology, Hoboken, NJ 07030, USA
E-mail: HDU@ATTILA.STEVENS-TECH.EDU

R. LARKER
Lulea University of Technology, Lulea S-97187, Sweden

Hot-isostatically pressed silicon oxynitride (Si_2N_2O) ceramics free from sintering aids were oxidized in 1 atm dry oxygen at 1100 and 1300 °C. The structural and chemical characteristics of the oxide and the nature of the oxide–Si_2N_2O interface were determined using cross-sectional transmission electron microscopy in conjunction with small-probe energy dispersive X-ray analysis and selected-area electron diffraction. Oxidation of Si_2N_2O resulted in the formation of amorphous SiO_2. The oxide–Si_2N_2O interface was chemically abrupt. The interface was very flat when parallel to low-index, high atomic density Si_2N_2O crystal planes but became notably undulated if oriented to high index, low atomic density planes. About 6 vol% residual SiO_2 phase was present in the bulk of the Si_2N_2O ceramics. Current results have provided an important baseline for the understanding of the oxidation behaviour of Si_2N_2O. © *1998 Kluwer Academic Publishers*

1. Introduction

Silicon oxynitride (Si_2N_2O) ceramics have attracted great technological interest because of the prospects they offer for high-temperature structural applications [1–5]. The main advantage of Si_2N_2O has been its good resistance to oxidation and to molten non-ferrous metals and salts [6]. However, like other silicon-based ceramics such as silicon carbide (SiC) and silicon nitride (Si_3N_4), Si_2N_2O is thermodynamically unstable and will oxidize when exposed to an oxidizing environment. Oxidation and associated degradation processes can significantly limit the performance and long-term reliability of Si_2N_2O components in many projected applications. Further interest in the oxidation study of Si_2N_2O stems from the formation of a silicon oxynitride interlayer during oxidation of chemically vapour deposited (CVD) Si_3N_4, which plays mechanistic role in the oxidation of CVD Si_3N_4 [7–9]. A good knowledge of the oxidation behaviour of Si_2N_2O will also help enhance the understanding of the oxidation mechanism of Si_3N_4.

Documented studies of oxidation of pure Si_2N_2O ceramics have been focused mainly on the kinetic aspects of the oxidation process [3, 4, 10]. Persson *et al.* [10] studied the oxidation rate of hot isostatically pressed (HIPed) Si_2N_2O without sintering aids at 1300–1600 °C in flowing oxygen using the thermogravimetric analysis technique. A parabolic rate law was followed below 1350 °C where the oxide scale was silica and above 1500 °C where the oxide was cristobalite. At 1350–1500 °C where the oxide layer was only partially crystallized, a non-parabolic weight gain was observed. The kinetic analysis by Persson *et al.* [10] was very extensive but their characterization of the oxidized samples relied only on scanning electron microscopy and X-ray diffraction, which may not reveal sufficient details. O'Meara *et al.* [11] studied the oxidation of pressureless sintered Si_2N_2O with Y_2O_3 and Al_2O_3 as sintering aids in the temperature range 1000–1500 °C. This material was shown to have excellent oxidation resistance. Detailed analysis using transmission electron microscopy revealed that the oxide developed a duplex morphology. The inner region is amorphous, rich in additive and impurity cations, and the outer region consisted of $Y_2Si_2O_7$ crystals embedded in a silicon-rich glassy phase.

There is a dearth of information on the structural and chemical characteristics of the oxide layer formed on Si_2N_2O ceramics free of impurities and additives, and on the nature of the oxide–Si_2N_2O interface. Such a knowledge will constitute an important baseline for accurate interpretation of oxidation kinetic data and for an atomistic understanding of the oxidation mechanism. The main goal of this study was to examine in detail the structural, chemical and interface characteristics of the oxide grown on the purest available Si_2N_2O. Many analytical techniques were employed in this investigation which include cross-sectional

transmission electron microscopy (TEM), selected-area electron diffraction (SAD), and energy dispersive X-ray analysis (EDX). Scanning electron microscopy (SEM) was also used in conjunction with chemical etching experiments.

2. Experimental procedure

Polycrystalline Si_2N_2O ceramics used in this study were produced by hot isostatic pressing from mixtures of equal molar amounts of high-purity Si_3N_4 and SiO_2 powders with no sintering additives at 1900 °C. A detailed description of the processing conditions was provided elsewhere [5]. X-ray diffraction analysis indicated that the sample materials consist of 96% crystalline Si_2N_2O, 2% α-Si_3N_4, and 2% β-Si_3N_4 (in weight). The diffraction pattern for Si_2N_2O matches well with JCPDS File 33-1162 [12]. Plate samples cut from the Si_2N_2O rods were polished to 0.25 μm mirror finish using various grades of diamond paste. The samples were ultrasonically cleaned in deionized water, acetone, and methanol to remove surface contamination before oxidation. Oxidation experiments on the Si_2N_2O samples were carried out in a $MoSi_2$-heated Al_2O_3-tube furnace in 1 atm dry oxygen flowing at 100 standard cm min^{-1}. The samples were oxidized at 1100 °C for 8 and 16 h and 1300 °C for 3 and 6 h.

In the process of TEM specimen preparation, two oxidized Si_2N_2O samples were glued together face-to-face using M-610 epoxy glue and were subsequently cut to thin slices of less than 1 mm width. Mechanical grinding using the tripod technique was employed in order to achieve an ultimate thinness at the edge of the cross-section of about 0.1 μm. Further thinning was done by argon ion milling at 5 kV and 15° incident angle for approximately 30 min.

The cross-section thin foils were investigated in a Jeol 2010 transmission electron microscope in order to study the structural, chemical and interface characteristics of the oxide layers on Si_2N_2O. The Jeol 2010 has a capability of high-resolution lattice imaging with a point-to-point resolution of 0.194 nm. The microscope is also equipped with a Gatan slow scan camera (SSC) and a Link ISIS EDX system using a small electron probe of 0.5 nm for elemental chemical analysis. The morphological features of the Si_2N_2O samples before and after oxidation were studied by a Jeol 840 scanning electron microscope with a 4 nm resolution in conjunction with preferential chemical etching of the oxide over Si_2N_2O in NH_4F: HF(10:1) solution.

3. Results

Bright-field TEM images of the Si_2N_2O samples oxidized at 1100 °C for 8 and 16 h are presented in Fig. 1a and b, respectively. The regions of light contrast correspond to the oxide phase as marked. Morphological waviness of the oxide–substrate interface was observed in both figures due to some initial roughness of the Si_2N_2O substrate. Based upon the TEM work, the 1100 °C/8 h and 1100 °C/16 h oxidation produced a ~120 nm and a ~200 nm oxide layer, respectively.

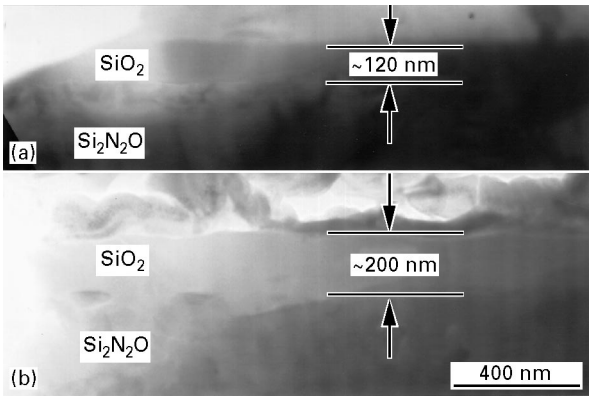

Figure 1 XTEM images of Si_2N_2O oxidized at 1100 °C for (a) 8 h, and (b) 16 h.

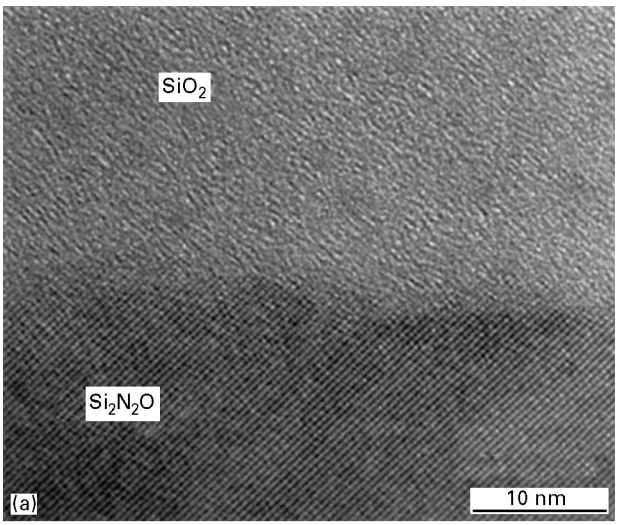

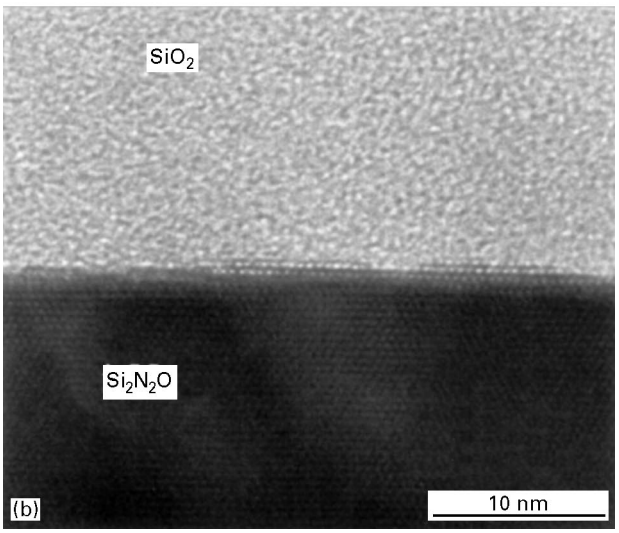

Figure 2 HRTEM images of Si_2N_2O oxidized at 1100 °C for 8 h delineating (a) the (1 1 1) Si_2N_2O–oxide, and (b) the (1 0 0) Si_2N_2O–oxide interfaces.

The features at the top of the oxide layer in Fig. 1b were identified as glue remnant.

Shown in Fig. 2 are high-resolution electron micrographs from the oxide–Si_2N_2O interface regions of the 1100 °C/8 h oxidized sample. Light contrast portions

of the images correspond to the oxide region. Fig. 2a and b delineate the interfacial morphology resulted from oxidation of the Si_2N_2O grains of different crystallographic orientations in the sample. The Si_2N_2O crystal lattice planes were indexed based on the interplanar spacings given in Fig. 2a and b. Direct comparisons were made with JCPDS File 33-1162 [12] and the well established X-ray diffraction data for Si_2N_2O by Idrestedt and Brosset [13] and Larker [5].

Specifically, the inclined lattice fringes in Fig. 2a were determined to represent the (0 0 1) plane whereas the interface plane can be either (1 1 1) or a plane of high indices such as (0 2 2), (5 1 3) or (3 3 3). Interface waviness in Fig. 2a precluded exact determination of the interface plane and orientation. Interesting features in Fig. 2a are the interface undulation and the apparent extension of the lattice fringes into the oxide region. The micrograph in Fig. 2b depicts the oxide–Si_2N_2O interface region with the (1 0 0) Si_2N_2O plane parallel to [0 0 1] zone axis. The oxide–(1 0 0) Si_2N_2O interface is very flat with a morphological overlapping of only about 0.7 nm.

Shown in Fig. 3a is the SAD pattern from the oxide region (Fig. 2) of the 1100 °C/8 h oxidized sample. The large and diffused pattern in this figure clearly indicates the amorphous nature of the oxide. As shown in Fig. 3b, EDX analysis using a 0.5 nm probe size revealed the presence of only silicon and oxygen in the oxide region. Nitrogen could not be detected (detection limit $\sim$0.1 at %) in the oxide region. Similarly, EDX analysis in the oxide region of proximity less than 1 nm from the oxide–Si_2N_2O interface also yielded no detectable nitrogen. Carbon traces were detected by EDX, which can be attributed to contamination of the analysing chamber by residual hydrocarbon molecules from the pump oil.

Presented in Fig. 4a is the SAD pattern ([$\bar{1}$ 0 1] zone axis) from the substrate region (Fig. 2). The diffraction spots correspond to several crystallographic planes in Si_2N_2O. The EDX spectrum taken from the substrate region in the immediate vicinity of the oxide–Si_2N_2O interface (proximity about 1 nm), as shown in Fig. 4b, showed the presence of silicon, nitrogen and oxygen, the constituent elements of Si_2N_2O. The same result was obtained in the matrix of the substrate region. SAD and EDX analysis of the 1100 °C/16 h oxidized sample produced results similar to the 1100 °C/8 h one.

Depicted in Fig. 5a and b are bright-field transmission electron micrographs of the Si_2N_2O samples oxidized at 1300 °C for 3 and 6 h, respectively. The regions corresponding to the oxide and the substrate, as marked in the figures, were determined from image contrast and based upon SAD and EDX analysis. The oxide thickness was measured to be around 420 and 780 nm for the 1300 °C/3 h and the 1300 °C/6 h oxidized samples, respectively. The SADand EDX results of these samples (not presented here) resembled those of the 1100 °C oxidized samples in terms of the oxide and interface characteristics.

In addition, TEM analysis revealed the presence of SiO_2 as inclusions or at the triple grain junctions in the Si_2N_2O substrate. Such features are depicted in the transmission electron micrographs shown in Fig. 6, which were taken from different regions of the same Si_2N_2O sample oxidized at 1100 °C for 8 h. The surface oxide layer is indicated with a thickness of $\sim$120 nm and the Si_2N_2O region is marked. The feature at the top of the oxide layer is from remnant glue. The oxide exhibited a lighter contrast in Fig. 6a than in Fig. 6b due to the relatively thin region examined. Phase and structural identification was provided by SAD and EDX analysis.

Fig. 6a illustrates a wedge-shaped cross-section of an amorphous SiO_2 inclusion in the near-surface region of the Si_2N_2O substrate. This inclusion penetrated from the base line of the oxide–Si_2N_2O interface to the substrate in a length scale of $\sim$750 nm

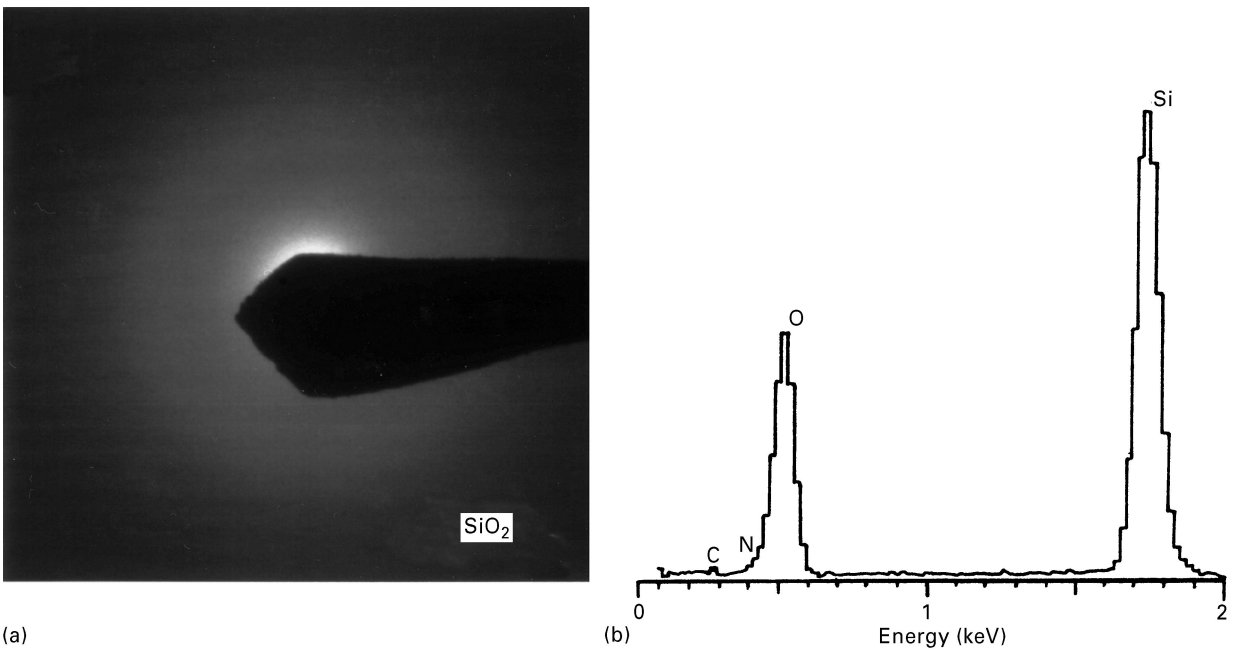

Figure 3 (a) SAD pattern, and (b) EDX spectrum obtained from the oxide region in Fig. 2.

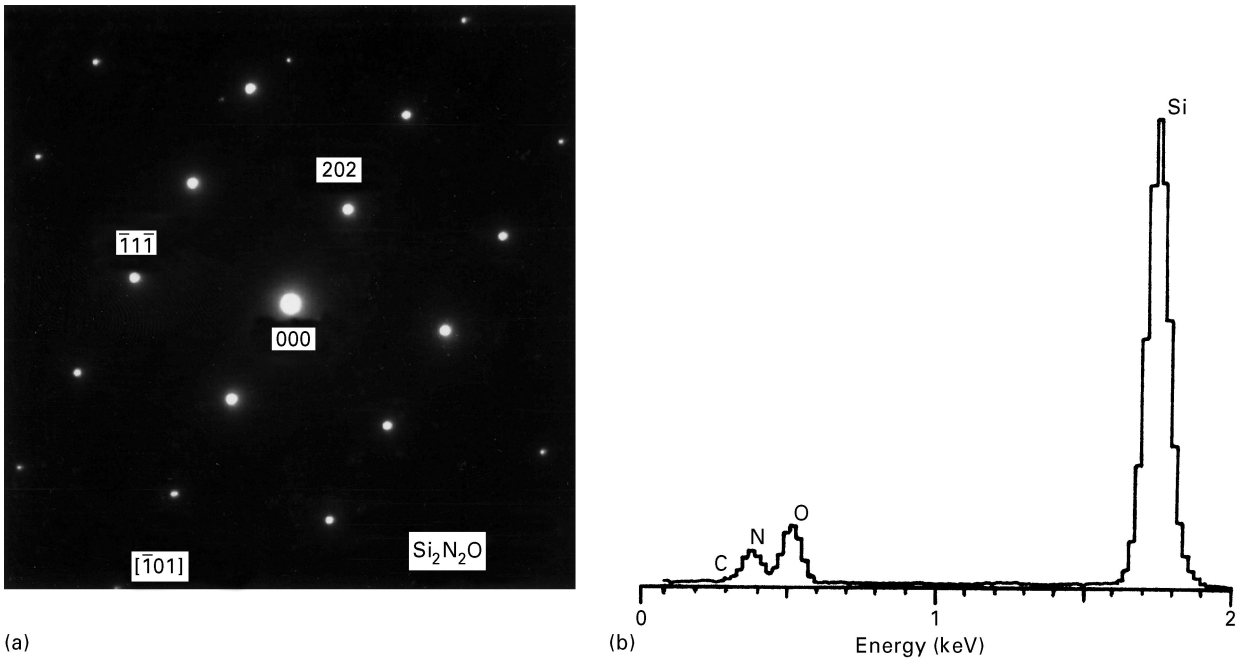

Figure 4 (a) SAD pattern, and (b) EDX spectrum taken from the substrate region shown in Fig. 2, in the immediate vicinity of the oxide–Si_2N_2O interface.

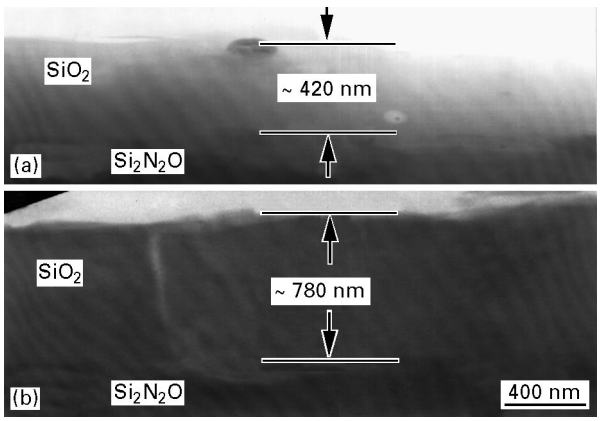

Figure 5 XTEM images of Si_2N_2O oxidized at 1300 °C for (a) 3 h, and (b) 6 h.

and formed a very flat boundary with the adjacent Si_2N_2O grains. The arrow in Fig. 6b marks an amorphous SiO_2 phase present at the triple grain junction. A widened passage from the near-surface grain boundary to the triple grain junction can also be seen, which is due to grain-boundary oxidation. Grain boundaries further away from the surface (such as the one near the bottom of Fig. 6b were generally found to be very narrow and free from detectable second-phase formation. The dark spherical inclusions within the Si_2N_2O crystal shown in Fig. 6b were rich in silicon and oxygen and exhibited some unknown crystalline features according to the SAD pattern. The band-like features of dark contrast in the Si_2N_2O phase were electron imaging artefacts such as thickness contours frequently observed in crystalline materials. These features are delineated during electron imaging as the result of thickness differences in the matrix or inclination of the grains with reference to the direction of the electron beam.

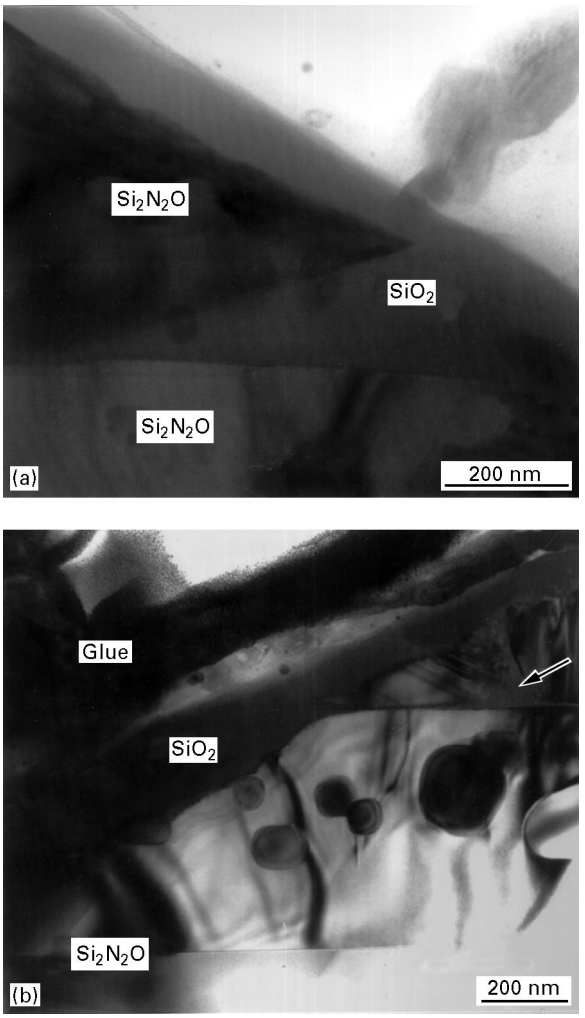

Figure 6 XTEM image of Si_2N_2O oxidized at 1100 °C for 8 h. Residual SiO_2 is incorporated (a) as inclusions in the Si_2N_2O matrix, and (b) at the triple grain junctions.

The presence of SiO_2 in the Si_2N_2O material was further confirmed by SEM in conjunction with chemical etching in the buffered HF solution, where the preferential removal of amorphous SiO_2 over crystalline Si_2N_2O was exploited. Shown in Fig. 7 are the scanning electron micrographs of the Si_2N_2O samples before and after 1100 °C/8 h oxidation and upon immersion in the HF solution. The surface of the Si_2N_2O sample not subject to HF treatment is featureless under SEM. The pores exposed in the unoxidized and etched sample (Fig. 7a) correspond to the sites of the SiO_2 inclusions in Si_2N_2O. The revealing of the grain structure besides the pores in the oxidized and etched sample (Fig. 7b) is an indication of grain-boundary oxidation in the surface region of the substrate. The SEM analysis is consistent with the TEM finding.

4. Discussion

Ample evidence was provided in this study that the oxide layer grown on Si_2N_2O at 1100 and 1300 °C is amorphous SiO_2 and the oxide–Si_2N_2O interface is structurally and chemically abrupt. There exists a strong correlation between interface morphology and the crystallographic orientation of the Si_2N_2O grains. In principle, crystal planes with high atomic density exhibit lower surface energy than those with low atomic density because of the small number of dangling bonds available for sharing with neighbour atoms. Furthermore, lattice planes of high crystallographic indices have small interplanar spacing and consequently low atomic density. The significant undulation of the interface shown in Fig. 2a is in contrast with the almost flat interface in Fig. 2b (undulations were about two atom layers). This morphological difference can be qualitatively explained in terms of interface energy associated with each surface plane.

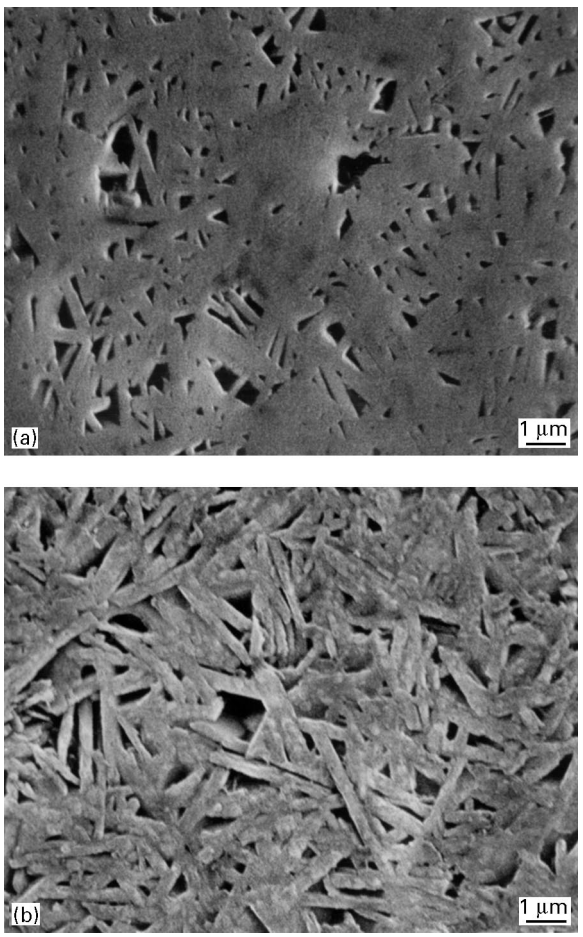

Figure 7 SEM images of HF-etched samples. (a) before, and (b) after oxidation, verifying the presence of SiO_2 in the Si_2N_2O matrix as indicated in Fig. 6.

Si_2N_2O has an orthorhombic structure with cell dimensions $a = 0.8868$ nm, $b = 0.5497$ nm, and $c = 0.4854$ nm and space group $Cmc2_1$ [5]. The atomic positions in Si_2N_2O are given by Idrestedt and Brosset [13, 14]. Based on the known lattice parameters, the planar atomic density for silicon, nitrogen and oxygen can be calculated at the interface. For example, the atomic density of the (1 0 0) interface plane (as in the case shown in Fig. 2b is 1.49×10^{15} Si atoms cm^{-2}. The atomic density of the (1 1 1) plane (a possible interface plane shown in Fig. 2a is only 0.74×10^{15} Si atoms cm^{-2}. Other possible planes of high indices are expected to have even lower silicon atomic densities. Similar correlations can also be found for nitrogen and oxygen. Therefore, the low surface energy of the atomically dense (1 0 0) Si_2N_2O interface plane in Fig. 2b may be the cause of the smooth morphology of the oxide–substrate interface as compared with the observed waviness in Fig. 2a which mainly resulted from exposure of low atomic density planes. Similar observations have been documented by Akatsu and Odhomari [15] in the studies of the Si–SiO_2 interface in terms of the relationship between the oxide–substrate interface morphology and substrate orientation. The (1 1 1) Si/SiO_2 interface (0.78×10^{15} Si atoms cm^{-2} on (1 1 1) Si) is extremely flat as opposed to the significant roughening of the (1 0 0) Si/SiO_2 interface (0.68×10^{15} Si atoms cm^{-2} on (1 0 0) Si).

Initial roughness of the Si_2N_2O substrate may also contribute to the undulation of the oxide–substrate interface shown in Fig. 2a. Such contribution is expected to be significant only at a significantly larger length scale. The roughness and location of the Si_2N_2O/SiO_2 interface in Fig. 2a could not be accurately determined because the crystalline Si_2N_2O was superimposed with the amorphous oxide along the electron beam path due to the finite interface roughness. Similar overlapping of crystalline silicon with amorphous SiO_2 was reported by Ross and Stobbs [16] which made the interface location indistinguishable.

In addition to surface oxidation, oxidation occurred in the grain boundaries near the substrate surface, as revealed by TEM and SEM. This observation can be explained based on the fact that grain boundaries are highly defective regions. They are fast diffusion channels for mass transport and are thus susceptible to oxidation. The grain-boundary oxidation was limited to the regions in the immediate vicinity of the substrate surface.

There is clear evidence for the presence of SiO_2 as inclusions and at the triple grain junctions in the as-received Si_2N_2O. Their amount was estimated to

be ~6 vol % from the SEM measurements. This is apparently due to incomplete conversion of the initial SiO_2 phase into the desired Si_2N_2O product. Additional support for this argument is the fact that 2 % α-Si_3N_4 and 2 % β-Si_3N_4 are present in the Si_2N_2O sample material HIPed from a mixture of equal molar amounts of Si_3N_4 and SiO_2 powders. Based on chemical stoichiometry, full conversion to Si_2N_2O should leave neither Si_3N_4 nor SiO_2 as a second phase. Therefore, co-existence of Si_3N_4 and SiO_2 in the HIPed product is expected. An intriguing and somewhat puzzling finding in the current investigation is that the residual SiO_2 in the Si_2N_2O ceramics HIPed at 1900 °C remained mostly amorphous. This is the principal reason why the early X-ray diffraction work [5] on this material did not yield the phase and compositional information on SiO_2. In contrast, only the α- and β-Si_3N_4 phases were revealed.

Our electron microscopy study revealed that oxidation of Si_2N_2O leads to the formation of a distinct SiO_2 amorphous layer. This investigation complements significantly the documented work on oxidation of Si_2N_2O with respect to the characteristics of the oxide layer and the oxide–Si_2N_2O interface. The details revealed form an important knowledge base for the understanding of the intrinsic oxidation behaviour of Si_2N_2O. It can be stated with certainty that oxidation of Si_2N_2O takes place by the advancement of a distinct SiO_2–Si_2N_2O interface. The Deal and Grove model [17] can be used to describe the kinetics of oxidation which leads to amorphous SiO_2.

The characteristics of the oxide and oxide–substrate interface on Si_2N_2O are quite similar to those of oxidized silicon and SiC [18–20]. The oxidation character of Si_2N_2O forms a sharp contrast with CVD Si_3N_4. Detailed characterization [7, 21–23] yielded strong evidence that oxidation of CVD Si_3N_4 results in the formation of a duplex oxide layer consisting of a SiO_2 outer layer and a SiN_xO_y inner layer. Du *et al.* [7, 8] proposed that oxidation of CVD Si_3N_4 takes place at two growth fronts: the SiO_2–"Si_2N_2O" and "Si_2N_2O"–Si_3N_4 interfaces. The formation of "Si_2N_2O" of a considerable length scale is possible only through continuous oxidation of Si_3N_4 at the "Si_2N_2O"–Si_3N_4 interface [7, 8, 24]. The oxidant at this reaction interface is supplied via inward diffusion through the "Si_2N_2O" layer, which is believed to be the rate-limiting mechanism. This model description was modified by Ogbuji *et al.* [21–23] in light of the better understanding of the characteristics of the oxide interlayer. Principally, the inner layer is amorphous in nature and has a composition ranging from SiO_2 near the oxide outer layer to Si_3N_4 near the substrate. Current investigation of the HIPed Si_2N_2O ceramics revealed no evidence of oxygen diffusion into the underlying Si_2N_2O substrate, which could lead to its gradual oxidation. The amorphous nature of SiN_xO_y inner layer, which has a more open structure compared to its crystalline counterpart, probably allows oxygen diffusion through this layer to take place and ultimately accounts for its existence during oxidation of CVD Si_3N_4. It is worth noting that a recent TEM study of oxidation of Si_3N_4 HIPed without sintering additives did not reveal the formation of SiN_xO_y as an intermediate oxide [25]. The oxidation behaviour of Si_3N_4 remains intriguing. Our on-going investigation of the oxidation kinetics of Si_2N_2O coupled with the acquired knowledge of the structural and chemical characteristics of the oxidized material will provide significant insights into the oxidation mechanism of Si_2N_2O and further enhance the understanding of the oxidation process of Si_3N_4.

5. Conclusion

This analytical study has revealed critical information on the structure and chemistry of the oxide layers grown on Si_2N_2O during high-temperature oxidation. The oxide layer formed consists of amorphous SiO_2. The chemical abruptness of the oxide–Si_2N_2O interface implies that oxidation of this material takes place via progressive advancement of the oxide–substrate interface. The morphology of the oxide–substrate interface can be flat or wavy, depending on the crystallographic orientations of the Si_2N_2O grains at the interface. Grain-boundary oxidation has been shown to take place but is confined in the near-surface region of the substrate. Residue and mostly amorphous SiO_2 is present as inclusions and at the triple grain junctions of the as-received Si_2N_2O ceramics. This phase is the remnant from the initial powder mixture used in the HIPing process.

Acknowledgements

This work was supported by the National Science Foundation under grant number DMR-9401856. The authors would like to thank Mr. Yongxiang Guo, Univeristy of New Mexico, for his assistance in the TEM work.

References

1. M. WASHBURN, *Am. Ceram. Soc. Bull.* **46** (1967) 667.
2. M. BILLY, P. BOCH, C. DUMAZEAU, J. C. GLANDUS and P. GOURSAT, *Ceram. Int.* **7** (1981) 13.
3. M. OHASHI, S. KANZAKI and H. TABATA, *J. Am. Ceram. Soc.* **74** (1991) 109.
4. P. GOURSAT, P. LORTHOLARY, T. TETARD and M. BILLY, in "Proceedings of the 7th International Symposium on Reactivity of Solids", edited by J. S. Anderson, M. W. Roberts and F. S. Stone (Halsted Press, New York, 1972) p. 315.
5. R. LARKER, *J. Am. Ceram. Soc.* **75** (1992) 62.
6. P. BOCH and J. C. GLANDUS, *J. Mater. Sci.* **14** (1979) 379.
7. H. DU, R. E. TRESSLER, K. E. SPEAR and C. G. PANTANO, *J. Electrochem. Soc.* **136** (1989) 1527.
8. H. DU, R. E. TRESSLER and K. E. SPEAR, *J. Electrochem. Soc.* **136** (1989) 3210.
9. L. U. J. T. OGBUJI, *J. Am. Ceram. Soc.* **75** (1992) 2995.
10. J. PERSSON, P. O. KALL and M. NYGREN, *ibid.* **75** (1992) 3377.
11. C. O'MEARA, J. SJOBERG, G. DUNLOP and R. POMPE, *J. Eur. Ceram. Soc.* **7** (1991) 369.
12. "*Powder Diffraction File* (*Inorganic Compounds*) ", Card No. 33-1162, (Joint Committee on Powder Diffraction Standards, Swarthmore, PA, 1977).
13. I. IDRESTEDT and C. BROSSET, *Act. Chem. Scand.* **18** (1964) 1879.

14. C. BROSSET and I. IDRESTEDT, *Nature* Vol. **201** (1964) 1211.
15. H. AKATSU and I. ODHOMARI, *Appl. Surf. Sci.* **41**/**42** (1989) 357.
16. F. M. ROSS and W. M. STOBBS, *Surf. Interface Anal.* **12** (1988) 35.
17. B. E. DEAL and A. S. GROVE, *J. Appl. Phys*, **36** (1965) 3770.
18. A. H. CARIM and R. SINCLAIR, *J. Electrochem. Soc.* **134** (1987) 741.
19. M. NIWA, M. MATSUMOTO, H. ISAWAKI, M. ONADA and R. SINCLAIR, *J. Electrochem. Soc.* **139** (1992) 901.
20. B. HORNETZ, H-J. MICHEL and J. HALBRITTER, *J. Mater. Res.* **9** (1994) 3088.
21. L. U. J. T. OGBUJI and J. L. SMIALEK, *J. Electrochem. Soc.* **138** (1991) L51.
22. L. U. J. T. OGBUJI, *ibid.* **138** (1991) L53.
23. Idem, *J. Am. Ceram. Soc.* **78** (1995) 1279.
24. H. DU, R. E. TRESSLER, K. E. SPEAR and M. WANG, *J. Mater. Sci. Lett.* **8** (1989) 1341.
25. M. BACKHAUS-RICOULT and Y. G. GOGOTSI, *J. Mater. Res.* **10** (1995) 2306.

Received 17 October 1996
and accepted 18 March 1998